Current Applied Physics 11 (2011) S36–S40

Contents lists available at ScienceDirect

Current Applied Physics

journal homepage: www.elsevier.com/locate/cap

Planar-type thermoelectric micro devices using ceramic catalytic combustor

Woosuck Shin*, Takaomi Nakashima, Maiko Nishibori, Noriya Izu, Toshio Itoh, Ichiro Matsubara

AMRI, AIST, Nagoya 463-8560, Japan

ARTICLE INFO

Article history:
Received 29 October 2010
Received in revised form
12 January 2011
Accepted 12 January 2011
Available online 23 July 2011

Keywords:
Thermoelectric
BiSbTe
Micro-generator
Seebeck
Thin films
Catalyst

ABSTRACT

Thin-film couples of BiSbTe and Pt were deposited by RF sputtering and patterned by lift-off technique to form thermopile structures. To fabricate a planar micro-TE-generator, 11 thermopiles are connected in series as an array and Pt-loaded alumina ceramic catalyst was deposited on the thermopile as a combustor layer. The combustion and TE performance of the generator was investigated flowing 3 v/v% hydrogen in air into the test chamber; the average temperature gradient of eleven thermopiles developed between the hot and cold junctions of thermopiles was 50.6 K, and 1.9 μW of power was generated.

1. Introduction

The advantages of thin film thermoelectric (TE) generators over other micro power sources are their simplicity and absence of moving parts, which make TE generators good targets for miniaturization. Furthermore, by using a catalytic combustor as a heat source, the problem of mechanical contact with the heat source is easily solved. Schaevitz et al. [1] first demonstrated the conversion of heat from the catalytic combustion of hydrogen into electrical power using a micro-TE-generator with a Pt thin-film combustor. The micro-generator operated at a temperature of 500 °C, and it produced a thermopile voltage of 7 V. Typical TE generators with a catalytic combustor [1,2] are composed of a catalytic combustor, a microheater, and a thermopile, on a thin membrane layer. The catalytic combustor provides thermal energy to the system to create a temperature gradient across the thermopile part. The thermopile converts a portion of this thermal energy reservoir into electrical energy.

A novel TE generator operating and self-igniting at room temperature without a heater has been demonstrated previously by the authors, with the help of the ceramic integration technology used for hydrogen sensors [3]. However, the generated power was very small, below the level of a microwatt, under a fuel gas of 3 v/v% H_2 in air [4], and both the integration of thermoelectric elements and the enhancement of thermoelectric materials are necessary. In micro power applications, the BiTe (N type) and BiSbTe (P type) thin films are the best candidate thin film materials, and can be prepared by various film preparation techniques, including co-deposition, the conventional RF-sputtering method [5,6], pulsed laser deposition (PLD) method [7], and electroplating [8] method.

The motivations for this work are to fabricate thermopile devices using BiSbTe thin films with the sputtering method, and to increase the power of the devices by integrating them as planar array devices. To improve device power, it is generally necessary to increase the number of thermopiles *n*. Since increasing *n* causes an increase of membrane size, and because the membrane is so fragile, distributing small membranes in a high packing density must be examined. When the membrane becomes small, the thermal resistance of the thermopile hot zone and cold heat sink can be reduced and, as a result, the thermopile n also affects the performance of the combustors. The degradation of the TE film performance during the process is also an important issue [9].

2. Experimental procedure

2.1. Thermoelectric thin film

P-type $Bi_{0.3}Sb_{1.7}Te_3$ (BST) bulk targets were prepared by using the hot press method and then used for RF sputtering. A post thermal annealing in Ar atmosphere was carried out to enhance the crystallinity of the films.

* Corresponding author.
E-mail address: w.shin@aist.go.jp (W. Shin).

1567-1739/$ – see front matter © 2011 Elsevier B.V. All rights reserved.
doi:10.1016/j.cap.2011.01.051

The crystalline orientation and the grain size of the films were characterized using X-ray diffraction (XRD). A commercial TE measurement system of RZ20001i (Ozawa science Co. Ltd.) modified for thin film measurements with 4-point pressure-contact electrodes [9] was used for the measurement of the conductivity, σ, and Seebeck coefficient, α, of the thin film samples.

2.2. Thermopile array device (TPAD)

We investigated the process parameters of the BST film, and the films for the TPAD were deposited with an RF power of 45 W, a substrate temperature of 140 °C, and in an Ar flow of 30 sccm. The post thermal annealing of the films was carried out at 300 °C for 30 min. Using the BST film and Pt film, a thermopile of thin-film couples of BST and Pt were patterned by lift-off technique. The devices were fabricated on double-side polished p-type silicon. Si_3N_4 was used as a dielectric membrane.

The substrate below the thermopile was etched out by bulk-Si wet etching. A wet etching window aligned to the front side patterns was fabricated on the reverse side of the substrate by the reactive ion etching (RIE) of the oxi-nitride multilayer, and wet etching was performed in an aqueous KOH solution. Details of the wet etching process were previously reported [3].

Fig. 1 shows the layout of the TPAD fabricated in this study. Eleven thermopile devices are integrated and connected in-series. Every thermopile structure consists of 10 (or 8) couples of BST-Pt connected in series and has its own membrane under the film pattern, and a TPAD consists of a total of $n = 102$ thermocouples. The area of a single membrane is 1.0×1.6 (or 1.3) mm^2, whereas the ceramic catalyst made of Pt-loaded alumina ceramic was deposited on the center of two BST-Pt thermopile line patterns, as a combustor layer.

The Pt lines are drawn up to the electrode pad pattern. The top passivation layer of SiO_2 was deposited by plasma enhanced chemical vapor deposition, PECVD, after the thermopile fabrication, to prevent current leakage across thermocouples. Finally, a Pt-Al_2O_3 catalyst line pattern was drawn on the center line of the thermopile.

The performance of the TPAD was investigated by infrared (IR) camera, flowing 3 v/v% H_2 in air into a test chamber, monitoring the output voltage, ΔV_{TPD}, and the average temperature gradient, ΔT_C, of eleven thermopiles in a single array developed between the hot and cold junctions of thermocouples.

3. Results and discussion

3.1. Thermoelectric thin film characterization

We have changed the process conditions of the films, using RF powers of 45 W, 70 W, and 100 W, and substrate temperatures of 140 °C, 200 °C, and 225 °C, and the best thermoelectric performance was obtained at low RF power and low substrate temperature, after annealing. Fig. 2 compares four typical X-ray diffraction (XRD) patterns of the BST thin films deposited at RF powers of 45 W and 70 W, before and after thermal annealing. The peak patterns of the as-deposited films were not clear and were of poor crystallinity, and those of the films annealed at 300 °C showed clear peak patterns of $Bi_{0.3}Sb_{1.7}Te_3$.

For the annealed films, the (00l) peaks are prominent, indicating that these films exhibited c-axis orientation as deposited on this dielectric top layer on the Si substrate. Considering the peak ratio of (006)/(015), with 45 W RF power, the film seems more c-axis oriented, and the RF power of 45 W was chosen for the device process.

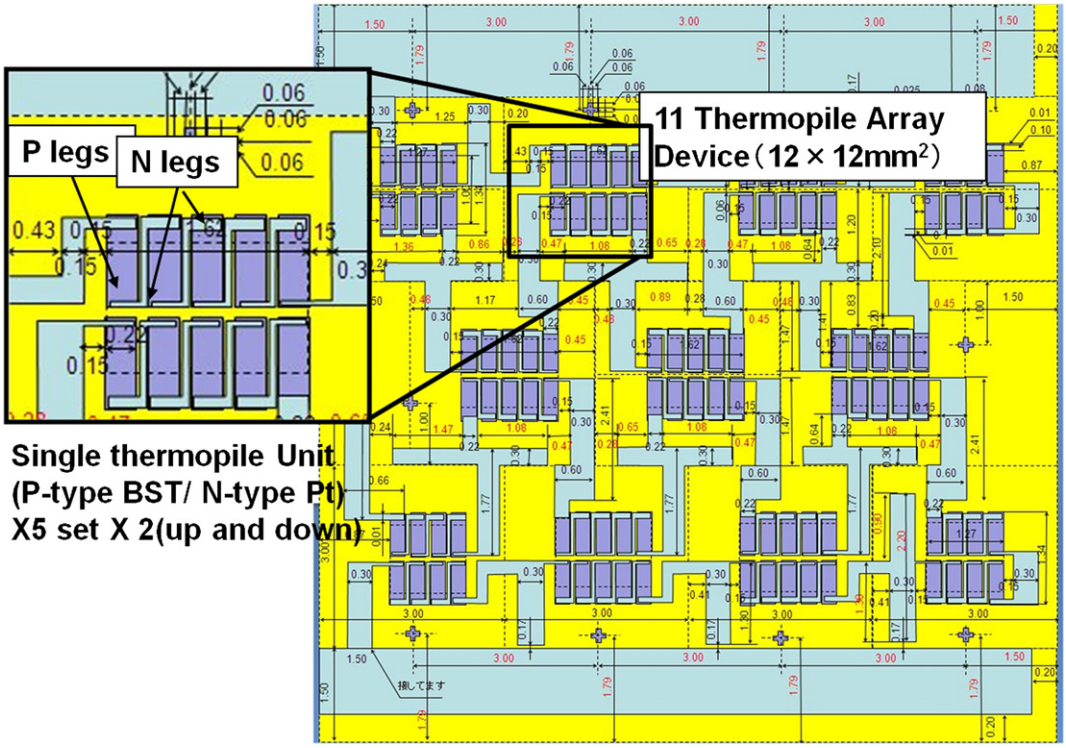

Fig. 1. Layout of Thermopile Array Device, TPAD. Single thermopile unit consists of a couple of thermocouple bundles, Pt N-type legs and BST P-type legs. As the Pt film is of low resistivity the width of the Pt leg is narrow and the electrode pad is also patterned by Pt film.

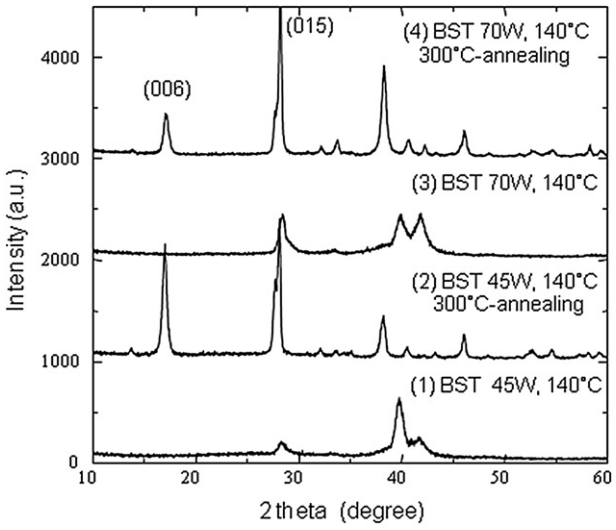

Fig. 2. XRD patterns of the sputter deposited BST thin films. The sputter deposited film was annealed at 300 °C for 30 min.

Fig. 3 shows the thermoelectric properties of the BST films deposited with an RF power of 45 W. The Seebeck coefficient, α, and the conductivity, σ, were measured up to 140 °C in air. The temperature dependencies of the σ measured in this range indicate that the as deposited film was semiconductor-like, and becomes close to metallic after annealing.

After annealing, the σ of the film increased by 3 times and became close to the reported bulk data. As a result, the *PF* of the film increased to over 10 times as high as 2.47×10^{-4} W/mK^2 at 140 °C, but was still lower than the value of 1.59×10^{-3} W/mK^2 reported by Takashiri et al. [5]. However, the TE data of the film are still small compared to the previous value reported by Obara et al. [7], whose film was the same level as those of optimized bulk. For example, the α was 200 μV/K. The properties in the principal can be determined by the crystallinity and carrier concentration. The Hall measurement data, carrier concentration and mobility of the BST films are plotted with respect to the temperature in Fig. 3(c). The XRD analysis shows that the annealing process seems to enhance the crystallinity of the film and to induce high carrier mobility, over 3 times increased. The higher carrier mobility is thought to lead to higher TE performance, and increase of both the α and σ are well understood. The carrier concentration seems to be of a sufficiently high level and to be unchanged by this annealing, and we can suggest no change in the defect structure such as a loss of Te element during the annealing.

3.2. Device test with catalytic combustion

Surface temperature evolution of the devices by the catalytic combustion reaction was explored with a high-speed thermal imaging system and temporal averaging technique to construct thermal images, i.e., the data set of the temperature, as shown in Fig. 4. The fabrication of the TPAD is based on micro-technology processes, and especially the process step of KOH etching, which is to release the membrane of the device, and is important for device yield. The backside of the device is shown in Fig. 4 (upper left snap) and the front side patterns and the catalyst lines are clearly shown (lower left). If the Si is partially etched, the backside of the membrane is not transparent but brown colored, and the catalyst could not combust the hydrogen effectively at room temperature.

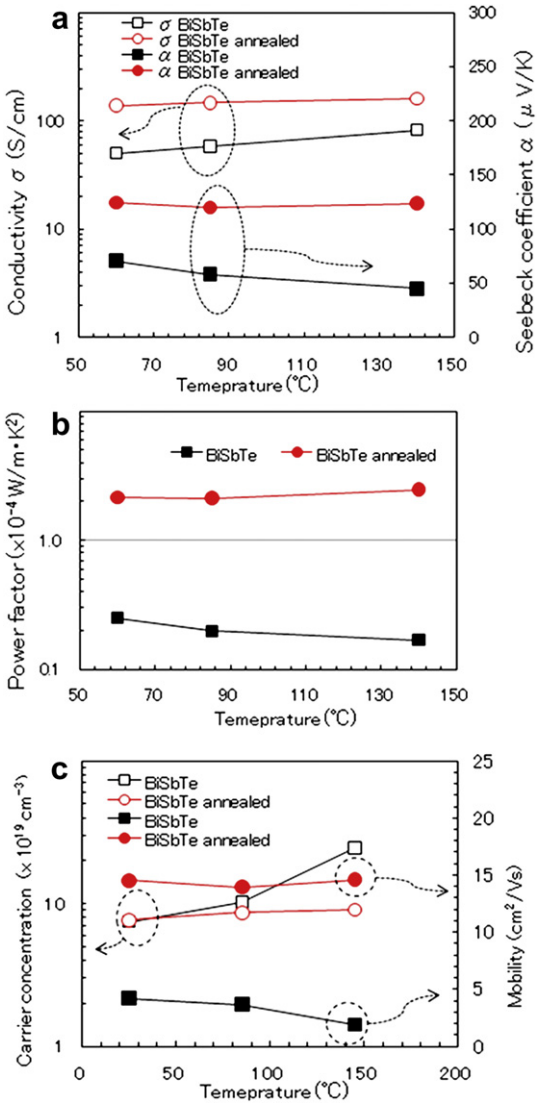

Fig. 3. Thermoelectric transport parameters of the BST films deposited on the Si_3N_4/SiO_2/Si substrate after thermal annealing; a) conductivity and Seebeck coefficient, b) power factor, *PF*, and c) carrier concentration and mobility.

Under the gas flow of 3 v/v% H_2 in air at the rate of 200 ccm, the catalyst combustor burnt the hydrogen and heated up one end part of the thermopile on the thermopile array device (TPAD). When the hydrogen gas was introduced and oxidation heat generated, the temperature at the center of the catalyst increased and the heat spread out from the catalyst on the membrane to the Si substrate rim through the thermopile, as shown in Fig. 5. One can observe that the temperature out of the catalyst pattern is almost the same and thermopile structure in this study has enough low thermal conductivity to confine the heat at the hot-side of the thermopile.

From these images, the temperature changes of the surface of the TPAD were monitored and the ΔT_C was calculated, and the voltage from the thermopile pattern, ΔV_{TPAD}, (the ΔT_C and the reading electrodes of ΔV_{TPAD} and ΔR_{TPAD} are indicated in Fig. 5) was simultaneously acquired, and the results are listed in Table 1.

The better the thermal conductivity of the thermopile line pattern, the lower the ΔT_C and the lower the ΔV_{TPD} that will be obtained. The ΔT_C of the thermopile array devices was smaller by 18 °C than the single thermopile device reported previously [10], which strongly depends on the shortened length of the

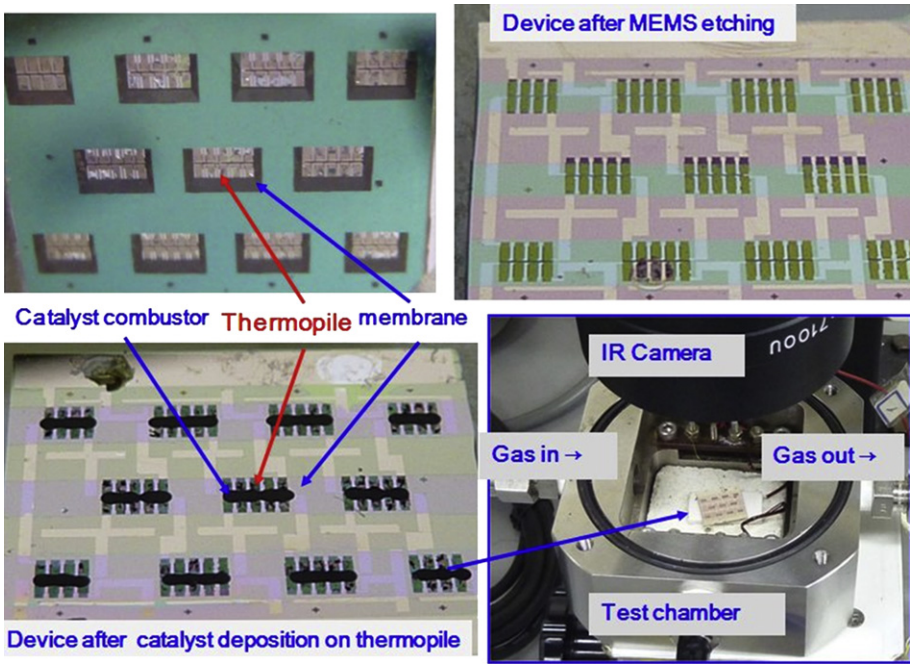

Fig. 4. TPAD with ceramic catalyst deposited on the center of BST-Pt thermopile line patterns set in the test chamber.

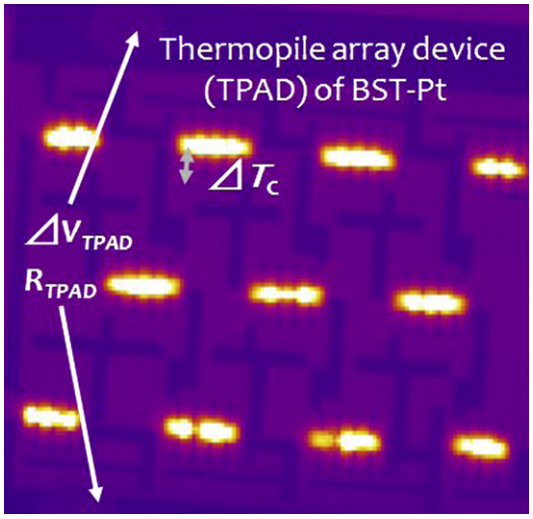

Fig. 5. Combustion of 3 v/v% H_2 in air gas by the Pt-Al_2O_3 catalyst on the thermopile array device (TPAD). A temperature differential was built up across the thermopile legs, and the voltage output and the resistance of the TPAD were recorded from the electrodes (indicated by arrows) during this combustion.

thermocouple legs of the TPAD. The enhanced performance is mainly due to the better performance of the TE film, especially the low resistivity, and the integration of 11 thermopiles increased the total power. The power density of the TPAD is 1.93 μW/1.44 cm^2 = 1.34 μW/cm^2, almost the same level as the previous thermopile device [10] using the same BST-Pt thermocouples.

A serious problem was that the apparent Seebeck coefficient of the BST and the Pt thin film couple of the TPAD was very small. The apparent Seebeck coefficient of α_{app} evaluated from the ΔT_C and ΔV_{TPD} divided by the number of couples, 102, was very much smaller than the sum of the α of the BST and Pt. The α_{app} of the TPAD was 41 μV/K smaller than the $\alpha_{BST} + \alpha_{Pt} = 100$ μV/K (the α of the Pt is −5.6 μV/K and −7.5 μV/K at 45 °C and 100 °C, respectively) at 45 °C (averaged temperature). As the resistance of the Pt lines was measured to be less than 100 Ω, the main contribution of the R_{TPD} is the resistance of the BST film patterns.

Considering the low resistivity value of the PLD BST films, as in Fig. 3, the low resistance level of the thermopile device was expected, but the resistance after the KOH process was not satisfactory. The R_{TPAD} of the device was reduced from 20 kΩ to 6 kΩ after the catalyst integration process. Because of the high Pt content (40 wt%) in the catalyst, the catalyst pattern is conductive, and the possible current leak can be suspected as the reason for the small α_{app}, even though the SiO_2 passivation layer is made between the thermocouple and catalyst of the TPAD in this study. A combustion test of the TPAD for very low gas concentration is currently being carried out, and combustion was found to be active down to 100 ppm H_2 in air, and the current leakage problem is under investigation.

Table 1
Combustion of H_2 gas by the Pt-Al_2O_3 catalyst on the TPAD. The resistance and the thermoelectric voltage produced by the temperature differential between the hot and cold zones of 11 thermopiles (102 thermocouples of BST-Pt film) are listed and compared to the single thermopile device* [10].

	Temp °C	ΔV_{TPD} mV	ΔT_c °C	α_{app} μV/K	R_{TPD} kΩ	P μW
Single TP*	25	128.12	68.3	156.3	22.98	0.179
11 TP array	25	213.3	50.6	41.3	5.89	1.931

References

[1] S.B. Schaevitz, A.J. Franz, K.F. Jensen, M.A. Schmidt, in: Proceedings of the 11th International Conference on Solid State Sensors and Actuators (2001), p. 30.
[2] A.M. Karim, J.A. Federici, D.G. Vlachos, J. Power Sources 179 (2008) 113–120.
[3] W. Shin, K. Tajima, Y. Choi, N. Izu, I. Matsubara, N. Murayama, Sens. Actuators, A 130–131 (2006) 411–418.
[4] M. Nishibori, W. Shin, K. Tajima, L.F. Houlet, N. Izu, T. Itoh, N. Murayama, I. Matsubara, Jpn. J. Appl. Phys. 45 (2006) L1130–L1132.
[5] M. Takashiri, T. Shirakawa, K. Miyazaki, H. Tsukamoto, Sens. Actuators, A 138 (2007) 329–334.
[6] H. Böttner, A. Schubert, K.H. Schlereth, D. Eberhard, A. Gavrikov, M. Jägle, G. Kühner, C. Künzel, J. Nurnus, G. Plescher, J. Microelectromech. Syst. 13 (2004) 414–420.

[7] H. Obara, S. Higomo, M. Ohta, A. Yamamoto, K. Ueno, T. Iida, Jpn. J. Appl. Phys. 48 (2009) 85506–85509.
[8] J.-P. Fleurial, G.J. Snyder, C.K. Huang, J. Herman, M.A. Ryan, N. Myung, J. Whitacre, in: Proceedings of the Symposium on Micropower and Microdevices, 2002–25, Electrochemical Society (2002), p. 215.
[9] W. Shin, M. Ishikawa, M. Nishibori, N. Izu, T. Itoh, I. Matsubara, Mater. Trans. 50 (2009) 1596–1602.
[10] W. Shin, T. Nakashima, M. Nishibori, T. Itoh, N. Izu, I. Matsubara, Y. Nakagawa, A. Yamamoto and H. Obara, J. Electron Mater. 40 (5) (2011) 817–822.